Research Article Vol. 30, No. 9 / 25 Apr 2022 / Optics Express 14651
Optics EXPRESS

Chiral biosensing using terahertz twisted chiral metamaterial

MIN ZHANG,[1] DANNI HAO,[1] SHUAI WANG,[1] RUI LI,[1] SHOU WANG,[1] YANQING MA,[1,2] RAMIRO MORO,[1] AND LEI MA[1,*]

[1]*Tianjin International Center for Nanoparticles and Nanosystems, Tianjin University, Tianjin, 300072, China*
[2]*State Key Laboratory of Precision Measuring Technology and Instruments, Tianjin University, 300072, Tianjin, China*
[*]*lei.ma@tju.edu.cn*

Abstract: Subwavelength chiral metamaterials with tunable geometries and compositions are essential to advance the development of chiral biochemical samples detection. Here, we report a spatial symmetry breaking chiral terahertz (THz) metamaterial structure with stacked layers of L-shape arranged gold disks as the periodic unit cell. The chiroptical response can be adjusted on-demand by manipulating the number of stacking layers and the twisted angle of the periodic unit between adjacent array layers. We reveal that the chiroptical response originates from the optical resonances of the gold disks and the adjacent gold disks array layers via experiments and numerical simulation analysis. Furthermore, we find that this chiral metamaterial can realize label-free detection of proline in biological samples and label-free enantio-discrimination of chiral molecules. The change of the analyte concentration can also regulate the transmission circular dichroism (TCD) intensity of the chiral metamaterials. Our results not only provide new ideas into the design of functional chiral metamaterials, but also bring new strategies to develop chiroptical biosensing devices.

1. Introduction

Chiral objects are common in our daily life. Many biological substances such as sugars, peptides, and amino acids are chiral and play important roles in medicine, biology, and chemistry [1–7]. The research of the chiral materials can be traced back to the 1890s, Bose experimentally demonstrated the optical properties of three-dimensional (3D) chiral materials for the first time [8]. Recently, THz chiral metamaterials with intriguing chiroptical properties have attracted wide attention in many emerging applications, such as chiral sensing and enantio-discrimination detection [9–15]. Same as chiral objects, chiral metamaterials appear in the form of mirror-symmetric enantiomers A and B, which cannot coincide with each other by simple rotation, scaling, or translation [16,17]. Structural chirality within metamaterials results in anisotropic interaction with right-handed circularly polarized (RCP) and left-handed circularly polarized (LCP) electromagnetic waves [18–20]. The chiroptical response of chiral metamaterials usually depends on their composition and the arrangement of their periodic arrays [21–24]. In recent years, a large number of chiral metamaterials have been demonstrated to manipulate transmission circular dichroism (TCD) response [25–34]. As an example, the TCD can be adjusted by changing the thickness of the azimuthally graded-depth of the plasmonic metamaterials [10], or by changing the thickness of the interval film of the double-layer chiral metamaterial [35]. One of the most important characteristics of chiral metamaterial is that its asymmetry can be artificially changed, which could effectively enhance the TCD responses [36–38]. Conventional passive control methods of chiral metamaterials usually rely on changing the size of the structural unit or the thickness of the metamaterials, and a large number of chiral metamaterials have been reported to manipulation polarization conversion and optical activity by using conversion passive control methods [39–45].

#448735 https://doi.org/10.1364/OE.448735
Journal © 2022 Received 17 Nov 2021; revised 26 Feb 2022; accepted 28 Mar 2022; published 20 Apr 2022

Optics EXPRESS

However, the works related to the THz chiral biosensing of the chiral metamaterials have rarely been reported yet.

In this work, we studied a new type of chiral metamaterials with broken symmetry that could enhance TCD by using the synergy between twisted morphology and local plasmonic response. It consists of several layers of chiral periodic arrays, where each one has unit cells made of four gold disks with different radii arranged in an L-shape and is rotated by a twisted angle with respect to the next layer in the stack. In the THz regime, the geometry-dependent chiral optical activity of the unit cell was systematically investigated by sequentially changing the twist angle of helical stacks. The experimental results show that by stacking up four layers of chiral periodic arrays and superimposing the L-shaped units with a twisted angle of 22.5°, the TCD intensity of the proposed chiral metamaterials can reach a higher level. By using this new four-layer chiral metamaterial a sensing platform, we carried out quantitative concentration measurements of proline solution and label-free enantio-discrimination between its D- and L- enantiomers. We found that the TCD intensity of chiral metamaterials increases with the concentration of proline. This chiral metamaterial and associate study can support the design of THz polarization sensor that has great potential for quantitative detection and chiral discrimination of biological materials.

2. Structure and design

Figure 1 shows the proposed twisted and chiral metamaterial. Each layer of periodic unit is made up of four gold disks with different radii arranged in an L-shape. The size of the entire metamaterial array is 6.6 mm × 7.2 mm. The layered metamaterial structures are fabricated via photolithography on a 500 μm thick SiO_2. The disks are made of 40 nm-thick gold on a 5 nm chromium adhesion layer. Gold is used due to its large numbers of free electrons, which is essential for plasmon generation. The metamaterials are built in two enantiomer forms (A and B), as shown in Fig. 1. They are mirror images of each other relative to the *y*-*z* plane. This stacked form, going from one-layer to a four-layer can be obtained straightforwardly by the aforementioned photolithography technique. An 11 μm polyimide (PI) is spin-coated between each layer as a dielectric spacer as shown in Figs. S1 and S2. The preparation processes are described in detail in the supplementary. An optical microscope image is shown in Fig. 2(a).

COMSOL Multiphysics simulations show the electric field and surface current distributions of the chiral metamaterials. In the simulation, the permittivity of gold is set in the Drude model with a plasma frequency $\omega_p = 1.37 \times 10^{16}$rad/s and collision frequency $\omega_c = 4.07 \times 10^{13}$rad/s. The refractive index of SiO_2 is set to 2.2 [46,47]. The polyimide (PI) with 11 μm thickness was described by a dielectric constant of 2.93 with loss tangent delta of 0.044 [48]. The circularly polarized incident wave is perpendicular to the metamaterial surface.

The fabricated twisted chiral metamaterials are characterized by a transmission-type THz time-domain spectroscopy system (THz-TDS) as shown in Fig. S3. The femtosecond laser oscillator used for the broadband THz beam has a repetition rate of 80 MHz and is purchased from Coherent. The spectral bandwidth is set to 70 nm. The pulsed laser beam with 800 nm center wavelength is focused onto a photoconductive switch. The transmission coefficients for RCP and LCP waves and the TCD are converted from linear polarization with four wire-grid polarizers. This system has a bandwidth of 0.1 THz to 2.0 THz by Fourier transform. To avoid the effects of moisture in air, the entire system is purged with dry nitrogen during measurements.

Optics EXPRESS

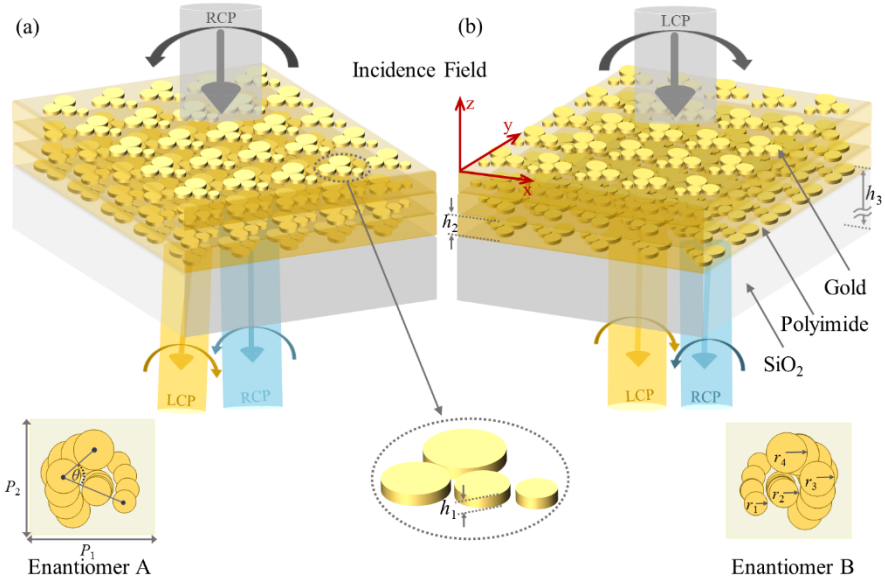

Fig. 1. Schematic drawing of the proposed four-layers chiral metamaterials for both enantiomers (A and B). They consist of L-shape arranged gold disks, and adjacent layers are separated by thin polyimide spacers. The incidence direction of the THz waves is along the indicated z-axis. (a) Enantiomer A. (b) Enantiomer B. Insets show the top views of A and B unit cells. Geometrical parameters are $P_1 = 240$ μm, $P_2 = 220$ μm, $r_1 = 25$ μm, $r_2 = 30$ μm, $r_3 = 35$ μm, $r_4 = 40$ μm, $h_1 = 45$ nm, $\theta = 63.15°$, $h_2 = 11$ μm and $h_3 = 500$ μm.

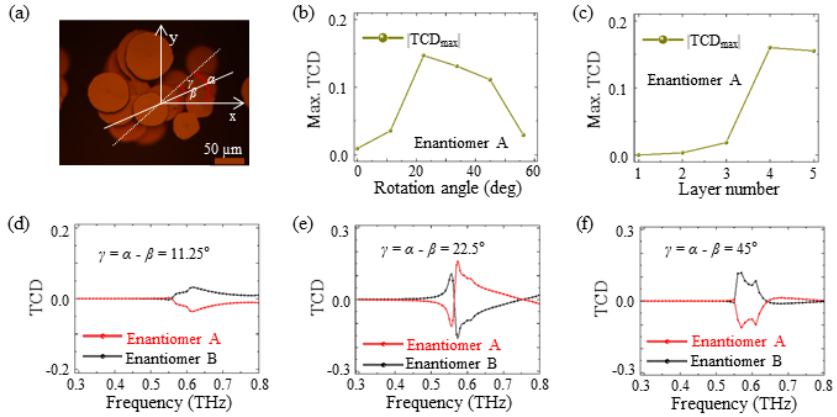

Fig. 2. Simulation results for proposed metamaterials. (a) Optical microscope image of the fabricated sample. (b) Maximum intensity of TCD as a function of twisted angle γ. (c) Maximum intensity of TCD as a function of the layers number of L-shape-arranged gold disks array. (d)-(f) TCD spectra under different twisted angles (γ =11.25°, 22.5°, 45°). The red and black lines are the results for enantiomer A and enantiomer B metamaterials, respectively.

Optics EXPRESS

3. Results and discussion

TCD is a parameter describing the difference between transmission coefficients of RCP and LCP waves. It is defined as

$$\mathrm{TCD} = \frac{T_{RCP} - T_{LCP}}{T_{RCP} + T_{LCP}} = \frac{(T_{++} + T_{+-}) - (T_{--} + T_{-+})}{(T_{++} + T_{+-}) + (T_{--} + T_{-+})} = \frac{(|t_{++}|^2 + |t_{+-}|^2) - (|t_{--}|^2 + |t_{-+}|^2)}{(|t_{++}|^2 + |t_{+-}|^2) + (|t_{--}|^2 + |t_{-+}|^2)}. \tag{1}$$

where T_{RCP} and T_{LCP} are the total transmittances of the metamaterials under RCP and LCP waves, T_{ij} is the i-polarized transmittances under j-polarized incidence with $\{i, j\} \in \{+, -\}$ and + representing RCP while – representing LCP. t_{ij} is the corresponding transmission coefficients. The data process is described in the supplementary

The TCD responses of the chiral metamaterials were first characterized using simulations. Figure 2(b) shows the simulated maximum intensity of TCD ($|\mathrm{TCD}_{max}|$ in the interested frequency rge of 0.5 to 0.6 THz) of the four-layer enantiomer A for varying twisted angles γ from 0 to 56.25° with a step of 11.25°, where γ is the twisted angle of the periodic unit between adjacent consecutive array layers. It is seen that the strongest TCD occurs at $\gamma = 22.5°$. Figures 2(d)–2(f) illustrate three TCD spectra of enantiomer A and enantiomer B with different γ. Due to the symmetry inversion, the RCP and LCP responses of enantiomer A will be equal to the LCP and RCP responses of enantiomer B. For a monolayer L-shape arranged gold disks array, the TCD is very weak, as shown in Fig. 2(c). ranging from 1 to 5 layers, as the layer number increases, the maximum intensity of TCD appears when the layer number equals 4.

In the following discussion, we focus on the THz polarization response of twisted four-layer enantiomer A excited by linearly polarized (LP) THz waves and circularly polarized (CP) THz waves. When the incident waves are LP, the polarization state of the transmitted wave changes owing to its broken symmetry. As shown in Fig. 3(a), there is a resonance at 0.46 THz under y-LP incidence, and a resonance at 0.58 THz under x-LP incidence. Then, we use polarization rotation angle (PRA) ψ and polarization ellipsoid angle (PEA) ε to characterize the polarization state conversions. They can be derived as follows [35]

$$\tan 2\psi = \tan 2\beta \cos\Delta\delta \tag{2}$$

$$\tan 2\varepsilon = \sin 2\beta \sin\Delta\delta \tag{3}$$

where $\tan\beta = T_x/T_y$, $\Delta\delta = \delta_x - \delta_y$. T_x and T_y are the transmission under two orthogonal LP incidence. δ_x and δ_y are the phases for two orthogonal LP signals. PRA represents the rotation angle of the polarization direction of the output wave relative to the incident wave. The positive value of PRA means that the rotation angle is clockwise direction, and the negative value means that the rotation angle is counterclockwise. PEA reflects the chirality ofhe output wave, that positive values mean right-handed rotation and the negative values mean left-handed rotation. As shown in Fig. 3(c), the peak values of PRA and PEA spectra are 44° and 15.6° at 0.51 THz, which means that the output wave exhibits right-handed rotation chirality with the rotation angle in the clockwise direction. When the incident waves are CP, we are more concerned about the chiroptical response. Figure 3(b) shows the polarization analysis of the transmission spectra in CP waves of the four-layers enantiomer A. Due to the asymmetry of the chiral structure unit cell, T_{++} and T_{-} are different. T_{++} spectrum has a trough at 0.46 THz, and T_{-} spectrum has a trough at 0.57 THz. Figure 3(d) shows the simulated and measured TCD spectra, the peaks of the TCD spectra are at 0.46 THz and 0.57 THz. Figure 3(e) shows experimental results of the evolution of the TCD along the increasing layer number of enantiomer A. It is found that the TCD gradually increases at 0.46 THz and 0.57 THz. The corresponding measured RCP and LCP transmissions can be seen in Fig. S4. Additional studies were performed to reveal the influence of the asymmetry of the L-shape units on the chiroptical responses. We compared the TCD

Optics EXPRESS

efficiency of gold disks with the same radius (r = 30 μm) in the four layers to the configuration with different radii (r_1 = 25 μm, r_2 = 30 μm, r_3 = 35 μm, r_4 . = 40 μm), as shown in Fig. 3(f). The metamaterial with the same radii has weak spatial asymmetry, which produces weaker chiral responses at 0.57 THz. Therefore, the strong TCD response efficiency in L-shape chiral metamaterials also originates from the spatial asymmetry of the unit cell.

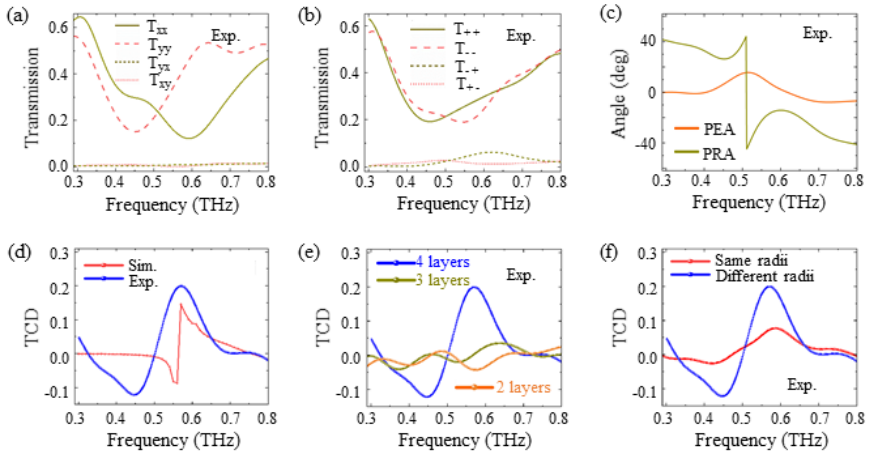

Fig. 3. Experimental results for proposed metamaterials in enantiomer A with twisted angle γ = 22.5°. (a) The co- and cross-polarized transmissions of the four-layers metamaterials under *x*- and *y*-polarized incidences. (b) The co- and cross-polarization transmissions of the four-layers metamaterials under RCP and LCP incidences. (c) PRA and PEA spectra of the four-layers metamaterials under two orthogonal linearly polarized incidences. (d) Experimental and simulated TCD spectra of the four-layers metamaterials under RCP and LCP incidences. (e) Experimental results of TCD spectra with the increasing number of L-shape-arranged gold layers (2, 3, and 4). (f) The TCD spectra comparison of the same radii (r_1 = r_2=r_3=r_4 = 30 μm) vs different radii (r_1 = 25 μm, r_2 = 30 μm, r_3 = 35 μm, r_4 = 40 μm) of four gold disks on four layers unit cells.

We analyze the electric field and surface current density distributions of enantiomer A at 0.57 THz when illuminated with CP waves, as shown in Fig. 4. The electric dipole moments induced by the flowing currents are illustrated with color scales for the electric field intensity distributions, and the red arrows indicate the direction of oscillating currents. For LCP incidence, the electric field intensities on the first to fourth layer reveal that the local plasmonic resonance could lead to strong electric field enhancement in the gap of the adjacent gold disks, which results in a transmission dip. For RCP incidence, the electric field intensity is much smaller than that of the LCP wave due to the spin-dependent coupling effect. Therefore, the spin-selectivity can be identified by the distribution of the electric field intensity corresponding to the resonance frequency and the coupling frequency of each layer. This difference in the distribution of electric fields between RCP and LCP waves corresponds to the TCD response. Figures 4(e) and 4(j) show the surface current density distributions at the bottom periodic unit cell. The currents flow in a helical pattern and generate the local plasmonic modes.

The above experimental results prove that by stacking up four layers of chiral periodic arrays and superimposing the L-shaped units with a twisted angle of 22.5°, the TCD intensity of the proposed chiral metamaterials can reach a higher level. Therefore, the chiral metamaterial sensors we will discuss next are all based on the chiral metamaterial with a twisted angle of 22.5° and four array layers. We demonstrated the chiral sensing capability of the four-layers twisted metamaterial using proline, which is an essential amino acid with a molecular weight of 115.13 g/mol. It has

Optics EXPRESS

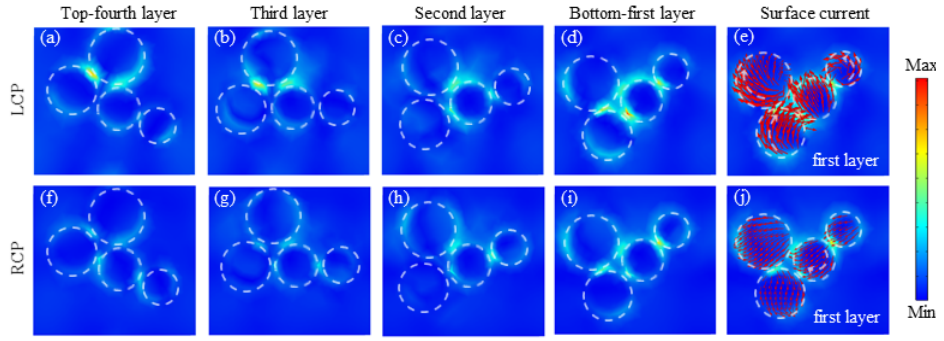

Fig. 4. Normalized electric field and surface current density distributions of enantiomer A under (a)-(e) LCP illumination and (f)-(j) RCP illumination from the first to the fourth layer at 0.57 THz. The electric field intensity distribution is indicated with red-green color scales, the red arrows indicate the surface current distribution.

two enantiomers, D-proline and L-proline. These two prolines are purchased from Damasbeta Company with purity of 99%. In the experiment, deionized water is used to prepare the proline solution with different concentrations. The volume of the proline solution added on the surface of the chiral metamaterials is 20 μL. The proline solution crystallized at the temperature of 60°C to form a proline film with a thickness of about 0.38 mm. Images of the crystallized biological samples on different substrates can be found in Fig. S7. We characterize the polarization states by PRA and PEA parameters. Figure 5(a) shows the experimental PRA spectra of the D-proline with different solution concentrations. All the peaks of PRA spectra reach to a maximum of 44° for each sample concentration, but the abrupt frequency corresponding to the peak values of PRA spectra red-shifted significantly with the increase of the D-proline concentration. Figure 5(b) shows the PEA spectra of the D-proline. The peak frequency moves to lower frequency with the increase of D-proline concentration. Figure 5(c) shows the PRA and PEA spectra of the D- and L-proline with the same solution concentrations, respectively, and the PRA or PEA spectra are almost the same around the abrupt frequency of 0.42 THz.

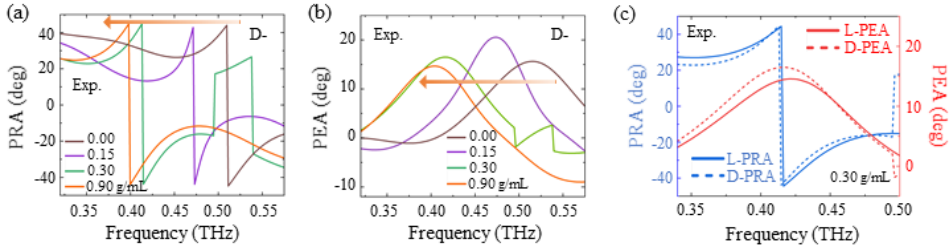

Fig. 5. Experimental sensing results of LP illumination on the chiral metamaterial sensor in enantiomer A. (a) PRA spectra, and (b) PEA spectra of D-proline solutions with different concentrations. c) PRA spectra and PEA spectra of D-proline and L-proline solutions at the concentration of 0.30 g/mL.

Although the above polarization conversion methods can be used to quantitatively determine the concentration of proline, it is difficult to distinguish D-proline and L-proline chiral enantiomers. As a result, we begin to study the chiroptical response of the proline sample on the four-layer twisted enantiomer A. In this case, the information carried by the amplitude and phase of the transmitted CP wave is essential to obtain the TCD spectra of the proline on the enantiomer A. Figure 6(a) shows the TCD spectra of chiral metamaterial without proline, D-proline on

Optics EXPRESS

SiO_2 substrate, and D-proline on chiral metamaterial, respectively. It can be seen that the chiral intensity of proline sample is very low in the absence of chiral metamaterial enhancement. The TCD spectra of D-proline with the chiral metamaterials are shown in Fig. 6(b), which indicates that the peak of the TCD spectra is at about 0.54 THz, and the peak redshifts while enhances as the D-proline concentration increases.

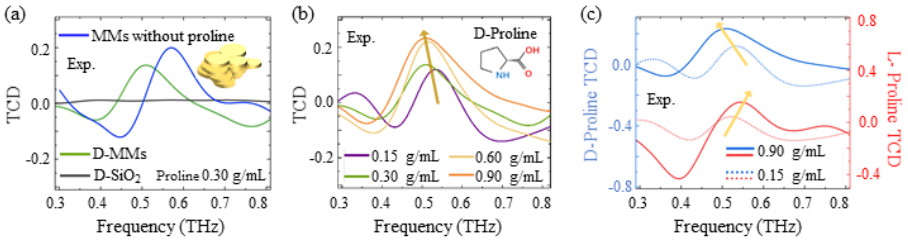

Fig. 6. Experimental chiral sensing results of CP illumination on the chiral metamaterial sensor in enantiomer A. (a) TCD spectra of chiral metamaterial without proline, D-proline with the SiO_2 substrate, and D-proline with the chiral metamaterials (MMs), respectively. (b) TCD spectra of D-proline solutions with different concentrations. (c) TCD spectra of D-proline and L-proline solutions with different concentrations. The inset in (a) shows metamaterials unit cells of enantiomer A, the inset in (b) is the structural formulas of D-proline.

Fig. S8(a) is an enlarged view of the black line in Fig. 6(a). From Fig. S8, it can be seen that the variation trend of the D-proline TCD intensity of the SiO_2 substrate is similar to that of the four-layer metamaterial in enantiomer A (blue line), indicating the similar chirality of the four-layer metamaterial enantiomer A and the D-proline sample. But their intensity is different. Therefore, the asymmetry of the metamaterial enantiomer A can be improved after being coated with D-proline [49,50]. The TCD spectra of D- and L-proline without metamaterial exhibit handedness-flipped chiroptical response [49]. The chirality of the four-layer metamaterial enantiomer A and the L-proline sample is opposite, thus the asymmetry of the metamaterial enantiomer A reduces after being coated with L-proline. We measured the peak of TCD spectra ($|\text{D-TCD}_{max}|$ and $|\text{L-TCD}_{max}|$ for D-proline and L-proline, respectively) on the four-layer metamaterial enantiomer A and calculated the dissymmetric factor $\Delta|\text{TCD}_{max}|=|\text{D-TCD}_{max}| - |\text{L-TCD}_{max}|$ at different concentrations (Fig. S9(a)). It can be seen the $\Delta|\text{TCD}_{max}|$ are positive, which means that the $|\text{TCD}_{max}|$ of D-proline is always larger than the L-proline at different concentrations, then, it is easy to distinguish the chiral enantiomers between D- and L-proline intuitively from the values of dissymmetric factor $\Delta|\text{TCD}_{max}|$. As shown in Fig. 6(c) and S9(b), we also see that there is a◦ prominent difference in chirality between two peaks for D- and L-proline within a certain frequency band. Due to the increased ratio of proline in a fixed volume of the proline solution expanded the proline film thickness, the peak frequency of TCD spectra is red-shifted significantly with the increase of D-proline concentration, while the peak frequency of TCD spectra is blue-shifted significantly with the increase of L-proline concentration. In order to verify its universality of the responses of such a design to other chiral molecule, the numerical simulations have been conducted [51], which nearly perfect reflect the experimental observations, details are included in the supplemental materials.

4. Conclusion

In summary, a new type of chiral metamaterial has been designed by twisting the unit cell of adjacent layers along the vertical axis with a certain angle to break the symmetries. Our

Optics EXPRESS

results show that the chiroptical activity can be tuned by adjusting the number of L-shape-arranged gold disk array layers and the twisted angle between the units of adjacent layers. In addition, we demonstrated the chirality sensing capability of the twisted chiral metamaterials using two enantiomers of proline as the biological sample analytes. This new four-layer chiral metamaterial sensor can distinguish D- and L-proline with label-free. The change of the proline concentration can also regulate the TCD intensity of the chiral metamaterials. These new THz chiral metamaterials and sensor devices pave the way to applications in chiral sensing and label-free enantioselective biosensing in the THz regime.

Funding. National Key Research and Development Program of China (2020YFC2004602); National Natural Science Foundation of China (11774255).

Acknowledgments. We would like to thank Dr. Kaiji Chen, Dr. Yihan Xu, Dr. Xueqian Zhang, Professor Zhen Tian and Professor Jiaguang Han for their help on part of measurements which were conducted in the Center for Terahertz Waves, Tianjin University.

Disclosures. The authors declare no conflicts interest.

Data availability. Data underlying the results presented in this paper are not publicly available at this time but can obtain from the authors upon reasonable request.

Supplemental document. See Supplement 1 for supporting content.

References

1. S. Yoo and Q. H. Park, "Chiral Light-Matter Interaction in Optical Resonators," Phys. Rev. Lett. **114**(20), 203003 (2015).
2. C. Bustamante, M. Maestre, and I. Tinoco, "Circular intensity differential scattering of light by helical structures. I. Theory," J. Chem. Phys. **73**(9), 4273–4281 (1980).
3. C. Bustamante, M. Maestre, and I. Tinoco, "Circular intensity differential scattering of light by helical structures. II. Applications," J. Chem. Phys. **73**(12), 6046–6055 (1980).
4. C. Bustamante, M. Maestre, and I. Tinoco, "Circular intensity differential scattering of light by helical structures. III. A general polarizability tensor and anomalous," J. Chem. Phys. **74**(9), 4839–4850 (1981).
5. G. Kenanakis, R. Zhao, N. Katsarakis, M. Kafesaki, C. M. Soukoulis, and E. N. Economou, "Optically controllable THz chiral metamaterials," Opt. Express **22**(10), 12149–12159 (2014).
6. J. Zhou, D. R. Chowdhury, R. Zhao, A. K. Azad, H. T. Chen, C. M. Soukoulis, A. J. Taylor, and J. F. Hara, "Terahertz chiral metamaterials with giant and dynamically tunable optical activity," Phys. Rev. B **86**(3), 035448 (2012).
7. S. S. Oh and O. Hess, "Chiral metamaterials: enhancement and control of optical activity and circular dichroism," Nano Convergence **2**(1), 24 (2015).
8. J. C. Bose and R. J. Strutt, "On the rotation of plane of polarisation of electric wave by a twisted structure," Proc. R. Soc. London **63**(389), 146–152 (1898).
9. W. Wu, W. Liu, Z. Chun, Y. Ling, J. Ding, X. Wang, L. Huang, and H. Li, "Optical rotation and electromagnetically induced transparency in a chiral metamaterial with C4 symmetry," Opt. Express **28**(20), 29496–29512 (2020).
10. M. Rajaei, J. Zeng, M. Albooyeh, M. Kamandi, M. Hanifeh, F. Capolino, and H. K. Wickramasinghe, "Giant Circular Dichroism at Visible Frequencies Enabled by Plasmonic Ramp-Shaped Nanostructures," ACS Photonics **6**(4), 924–931 (2019).
11. T. Petralli M, T. M. Wong, J. D. Byers, H. I. Yee, and J. M. Hicks, "Circular dichroism spectroscopy at interfaces: a surface second harmonic generation study," J. Phys. Chem. **97**(7), 1383–1388 (1993).
12. S. H. Lee, M. Choi, T. T. Kim, S. Lee, M. Liu, X. Yin, H. K. Choi, S. S. Lee, C. G. Choi, S. Y. Choi, X. Zhang, and B. Min, "Switching terahertz waves with gate-controlled active graphene metamaterials," Nat. Mater. **11**(11), 936–941 (2012).
13. Z. Xu, L. Xu, L. M. Liz, W. Ma, N. A. Kotov, L. Wang, H. Kuang, and C. Xu, "Sensitive Detection of Silver Ions Based on Chiroplasmonic Assemblies of Nanoparticles," Adv. Opt. Mater. **1**(9), 626–630 (2013).
14. Z. Xu, L. Xu, Y. Zhu, W. Ma, H. Kuang, L. Wang, and C. Xu, "Chirality based sensor for bisphenol A detection," Chem. Commun. **48**(46), 5760–5762 (2012).
15. Y. Huang, M. K. Nguyen, A. K. Natarajan, V. H. Nguyen, and A. Kuzyk, "A DNA Origami-Based Chiral Plasmonic Sensing Device," ACS Appl. Mater. Interfaces **10**(51), 44221–44225 (2018).
16. X. Shen, A. Asenjo, Q. Liu, Q. Jiang, F. J. Garcia de Abajo, N. Liu, N. Liu, and B. Ding, "Three-Dimensional Plasmonic Chiral Tetramers Assembled by DNA Origami," Nano Lett. **13**(5), 2128–2133 (2013).
17. L. Kang, S. P. Rodrigues, M. Taghinejad, S. Lan, K. T. Lee, Y. Liu, D. H. Werner, A. Urbas, and W. Cai, "Preserving Spin States upon Reflection: Linear and Nonlinear Responses of a Chiral Meta-Mirror," Nano Lett. **17**(11), 7102–7109 (2017).
18. P. Pachidis and V. E. Ferry, "Tunable optical chirality in a metamaterial platform with off-resonantly coupled metal-dielectric components," Opt. Express **26**(13), 17289–17299 (2018).

Optics EXPRESS

19. S. Sarkar, R. O. Behunin, and J. G. Gibbs, "Shape-Dependent, Chiro-optical Response of UV-Active, Nanohelix Metamaterials," Nano Lett. **19**(11), 8089–8096 (2019).
20. N. Yu and F. Capasso, "Flat optics with designer metasurfaces," Nat. Mater. **13**(2), 139–150 (2014).
21. S. Chen, F. Zeuner, M. Weismann, B. Reineke, G. Li, V. K. Valev, K. W. Cheah, N. C. Panoiu, T. Zentgraf, and S. Zhang, "Giant nonlinear optical activity of achiral origin in planar metasurfaces with quadratic and cubic nonlinearities," Adv. Mater. **28**(15), 2992–2999 (2016).
22. D. H. Kwon, P. L. Werner, and D. H. Werner, "Optical planar chiral metamaterial designs for strong circular dichroism and polarization rotation," Opt. Express **16**(16), 11802–11807 (2008).
23. P. Pachidis, B. M. Cote, and V. E. Ferry, "Tuning the Polarization and Directionality of Photoluminescence of Achiral Quantum Dot Films with Chiral Nanorod Dimer Arrays: Implications for Luminescent Applications," ACS Appl. Nano Mater. **2**(9), 5681–5687 (2019).
24. Y. Zhao, M. A. Belkin, and A. Alu, "Twisted optical metamaterials for planarized ultrathin broadband circular polarizers," Nat. Commun. **3**(1), 870 (2012).
25. C. Menzel, C. Rockstuhl, and F. Lederer, "An advanced Jones calculus for the classification of periodic metamaterials," Phys. Rev. A **82**(5), 053811 (2010).
26. Y. Huang, Z. Yao, Q. Wang, F. Hu, and X. Xu, "Coupling Tai Chi Chiral Metamaterials with Strong Optical Activity in Terahertz Region," Plasmonics **10**(4), 1005–1011 (2015).
27. G. Klos, M. Miola, and D. S. Sutherland, "Increased Refractive Index Sensitivity by Circular Dichroism Sensing through Reduced Substrate Effect," J. Phys. Chem. C **123**(12), 7347–7355 (2019).
28. L. Kang, C. Y. Wang, X. Guo, X. Ni, Z. Liu, and D. H. Werner, "Nonlinear Chiral Meta-Mirrors: Enabling Technology for Ultrafast Switching of Light Polarization," Nano Lett. **20**(3), 2047–2055 (2020).
29. Y. Chen, J. Gao, and X. Yang, "Chiral Metamaterials of Plasmonic Slanted Nanoapertures with Symmetry Breaking," Nano Lett. **18**(1), 520–527 (2018).
30. W. Ma, L. Xu, A. F. de Moura, X. Wu, H. Kuang, C. Xu, and N. A. Kotov, "Chiral Inorganic Nanostructures," Chem. Rev. **117**(12), 8041–8093 (2017).
31. S. Wang, L. Kang, and D. H. Werner, "Active Terahertz Chiral Metamaterials Based on Phase Transition of Vanadium Dioxide (VO2)," Sci. Rep. **8**(1), 189 (2018).
32. B. Yeom, H. Zhang, H. Zhang, J. I. Park, K. Kim, A. O. Govorov, and N. A. Kotov, "Chiral Plasmonic Nanostructures on Achiral Nanopillars," Nano Lett. **13**(11), 5277–5283 (2013).
33. B. Frank, X. Yin, M. Sch, J. Zhao, S. M. Hein, P. V. Braun, and H. Giessen, "Large-Area 3D Chiral Plasmonic Structures," ACS Nano **7**(7), 6321–6329 (2013).
34. M. Kuwata, N. Saito, Y. Ino, M. Kauranen, and Y. Svirko, "Giant Optical Activity in Quasi-Two-Dimensional Planar Nanostructures," Phys. Rev. Lett. **95**(22), 227401 (2005).
35. Z.-Y. Zhang, F. Fan, T.-F. Li, Y.-Y. Ji, and S.-J. Chang, "Terahertz polarization conversion and sensing with double-layer chiral metasurface," Chin. Phys. B **29**(7), 078707 (2020).
36. W. Liu, W. Wu, L. Huang, Y. Ling, C. Ba, S. Li, Z. Chun, and H. Li, "Dual-band asymmetric optical transmission of both linearly and circularly polarized waves using bilayer coupled complementary chiral metasurface," Opt. Express **27**(23), 33399–33411 (2019).
37. Y. Huang, X. Xie, M. Pu, Y. Guo, M. Xu, X. Ma, X. Li, and X. Luo, "Dual-Functional Metasurface toward Giant Linear and Circular Dichroism," Adv. Opt. Mater. **8**(11), 1902061 (2020).
38. Z. Wang, F. Cheng, T. Winsor, and Y. Liu, "Optical chiral metamaterials: a review of the fundamentals, fabrication methods and applications," Nanotechnology **27**(41), 412001 (2016).
39. J. K. Gansel, M. Thiel, M. S. Rill, M. Decker, K. Bade, V. Saile, G. von Freymann, S. Linden, and M. Wegener, "Gold Helix Photonic Metamaterial as Broadband Circular Polarizer," Science **325**(5947), 1513–1515 (2009).
40. Y. Tang and A. E. Cohen, "Enhanced Enantioselectivity in Excitation of Chiral Molecules by Superchiral Light," Science **332**(6027), 333–336 (2011).
41. Y. Wang, J. Xu, Y. Wang, and H. Chen, "Emerging chirality in nanoscience," Chem. Soc. Rev. **42**(7), 2930–2962 (2013).
42. X. Wu, L. Xu, L. Liu, W. Ma, H. Yin, H. Kuang, L. Wang, C. Xu, and N. A. Kotov, "Unexpected Chirality of Nanoparticle Dimers and Ultrasensitive Chiroplasmonic Bioanalysis," J. Am. Chem. Soc. **135**(49), 18629–18636 (2013).
43. C. L. Chen and N. L. Rosi, "Preparation of Unique 1-D Nanoparticle Superstructures and Tailoring their Structural Features," J. Am. Chem. Soc. **132**(20), 6902–6903 (2010).
44. S. J. Tan, M. J. Campolongo, D. Luo, and W. Cheng, "Building plasmonic nanostructures with DNA," Nat. Nanotechnol. **6**(5), 268–276 (2011).
45. K. L. Young, M. B. Ross, M. G. Blaber, M. Rycenga, M. R. Jones, C. Zhang, A. J. Senesi, B. Lee, G. C. Schatz, and C. A. Mirkin, "Using DNA to Design Plasmonic Metamaterials with Tunable Optical Properties," Adv. Mater. **26**(4), 653–659 (2014).
46. K. Seeger, "Microwave dielectric constants of silicon, gallium arsenide, and quartz," J. Appl. Phys. **63**(11), 5439–5443 (1988).
47. J. Kischkat, S. Peters, B. Gruska, M. Semtsiv, M. Chashnikova, M. Klinkmüller, O. Fedosenko, S. Machulik, A. Aleksandrova, G. Monastyrskyi, Y. Flores, and W. T. Masselink, "Mid-infrared optical properties of thin films

Optics EXPRESS

of aluminum oxide, titanium dioxide, silicon dioxide, aluminum nitride, and silicon nitride," Appl. Opt. **51**(28), 6789–6798 (2012).
48. M. Liu, E. Plum, H. Li, S. Li, Q. Xu, X. Zhang, C. Zhang, C. Zou, B. Jin, J. Han, and W. Zhang, "Temperature-Controlled Optical Activity and Negative Refractive Index," Adv. Funct. Mater. **31**(14), 2010249 (2021).
49. Z. Zhang, C. Zhong, F. Fan, G. Liu, and S. Chang, "Terahertz polarization and chirality sensing for amino acid solution based on chiral metasurface sensor," Sensors and Actuators B: Chemical **330**(1), 129315 (2021).
50. B. Yu, F. Zeng, Y. Yang, Q. Xing, A. Chechin, X. Xin, I. Zeylikovich, and R. R. Alfano, "Torsional Vibrational Modes of Tryptophan Studied by Terahertz Time-Domain Spectroscopy," Biophys. J. **86**(3), 1649–1654 (2004).
51. A. O. Govorov and Z. Fan, "Theory of chiral plasmonic nanostructures comprising metal nanocrystals and chiral molecular media," ChemPhysChem **13**(10), 2551–2560 (2012).